Performance Prediction of the Strong Company's Soft Ground Arrestor System using a Numerical Analysis

by Ernie Heymsfield
University of Arkansas
Department of Civil Engineering

October 2009

Sponsored by the
Mack Blackwell Transportation Center

Final Report

Department of Civil Engineering
Mack-Blackwell Rural Transportation Center

Acknowledgements

The research presented herein was conducted by the University of Arkansas Civil Engineering Department. The author is appreciative of the financial support provided by the Mack-Blackwell Transportation Center and The Strong Company. The contents of this report reflect the views and opinions of the author and do not necessarily reflect the views of the Mack-Blackwell Transportation Research Center or The Strong Company. The experimental work used in this study was conducted under the supervision of Dr. W. Micah Hale. The author recognizes Dr. James Yates for his assistance in the computer analysis included in this project. Special thanks go to Mr. Larry Porter of the Strong Company for his guidance during this project.

Performance Prediction of the Strong Company's Soft Ground Arrestor System using a Numerical Analysis

Abstract

Air transportation has an outstanding safety record; however, accidents do occur. Aircraft accidents can occur while the aircraft is at cruise altitude or during land movements: taxiing, takeoff, and landing. Overruns occur when an aircraft is unable to stop within the design runway length during landing or an aborted takeoff. In response, the Federal Aviation Administration (FAA) requires airfields to have a 1000-ft runway safety area (RSA) beyond the design runway length to provide additional runway length for an aircraft to stop during an overrun. However, some airports are unable to comply with this requirement due to either natural or man-made barriers that prohibit runway lengthening. In these cases, the FAA allows airport operators an alternative solution, a shorter runway safety area with a properly installed engineered material arrestor system (EMAS).

A sensitivity analysis is presented in this report showing the sensitivity of aircraft stopping distance to aircraft type, EMAS material, and EMAS configuration. A single bed configuration using an ideal low-density concrete material is used as a basis for the sensitivity study. Four aircraft types are considered in this study: B737-900ER, B747-400ER, B757-300, and the B767-400ER. A worse case scenario of zero reverse thrust with minimal tire-pavement friction is assumed. During the study, the development of the computer code, SGAS, was warranted in order to analyze the considered aircraft types. A methodology is also presented to develop aircraft parameters warranted in a stopping distance analysis using SGAS.

Table of Contents

List of Figures

List of Tables

Chapter 1
Introduction

Since the end of World War II, air transportation has experienced tremendous growth. Compared with the amount of air transportation growth, aircraft accidents have been very limited. Aircraft accidents can generally be categorized as occurring during flight at cruise altitude or during land operations: takeoff, landing, or taxiing.

The Federal Aviation Administration (FAA) conducted a survey of accidents and incidents occurring in the United States over the 1978-1987 ten-year period (David, 1990). The survey was specific to commercial aircraft takeoff and landing accidents/incidents. The survey reviewed over 500 accident/incident records. Two hundred and forty-six records could be categorized as: undershoot (18), landing off runway (11), veer-offs (97), overruns (33), and other (87). The "other" designation were events that the point of aircraft-ground impact occurred at a distance greater than 2000-ft (610 m) from the runway threshold or when during takeoff, the aircraft became airborne and then impacted the ground. Of the thirty-three commercial aircraft involved in an overrun, twenty-two occurred during landing and eleven during takeoff. Therefore, twice as many overruns occurred during landing as did during takeoff. All of the thirty-three aircraft involved in overruns stopped within 1600 ft (488 m) of the runway end. Thirty-one, 94%, stopped within 1000 ft (305 m) of the runway end. Approximately 90% of the overruns involved an aircraft with a 70 knots runway exit velocity or less (Federal Aviation Administration, 2005). In another study, Kirkland and Caves investigated overruns occurring between 1980-1998 (Kirkland and Caves, 2002). The study includes 180 civil aircraft overrun accidents/incidents occurring within the English-speaking world (Australia, Canada, United Kingdom, and the United States). Of the 180 events, 76% (137) occurred during landing while 24% (43) occurred during takeoff. The takeoff events primarily resulted from a late aborted takeoff. Twenty-two deaths and 37 seriously injured resulted from the 180 overruns. The fatalities and seriously injured were approximately equally distributed between landing and takeoff overruns. Kirkland and Caves found the average annual overrun rate within the study area to be approximately 2 overruns/year during takeoff, and 8 overruns/year during landing. A recently completed Airport Cooperative Research Program (ACRP) study examined

overrun and undershoot accidents/incidents to establish a database considering world regions with similar accident rates to the US: North America, Western Europe, Oceania, and limited Asian countries (Hall et al., 2008). Consequently, 459 accidents and incidents were considered in the database.

Factors influencing an aircraft accident/incident are: aircraft type, weather, airfield navigation system, runway dimensions, runway surface condition (wet, dry), runway surface treatment (grooved, porous friction surface), time interval between aircraft, time of day and pilot judgment. Overruns are more prone to occur during wet runway conditions.

In an effort to reduce the hazards of an aircraft overrun, the Federal Aviation Administration (FAA) requires a 1000 ft (305 m) runway safety area beyond the runway end (Federal Aviation Administration, 2005). However, in a report by Senator Frank R. Lautenberg's office, 507 commercial airport runways are deficient in meeting the 1000 ft (305 m) FAA runway safety area standards (Lautenberg 2006). Consequently, 325 of the nation's 573 major commercial airports have at least one inadequate runway. At many airports, satisfying the FAA runway safety area through runway extension is not feasible due to natural or man-made barriers. In these cases, the FAA permits an alternative solution by allowing an airport to implement an engineered materials arrestor system (EMAS). As of 2009, there are 41 EMAS installations at 28 U.S. airports (Federal Aviation Administration, 2009). An additional 17 installations are planned at 12 U.S. airports.

Five aircraft overruns have occurred at runways where an EMAS exists. Three of the overruns occurred at JFK International Airport in New York: May 1999, SAAB 340 commuter plane; May 2003, Gemini Air Cargo MD-11; and January 2005, Boeing 747. The fourth overrun involved a Mystere Falcon 900 occurring in July 2006 at Greenville Downtown Airport. The most recent overrun event occurred July 18, 2008 and involved a Mexicana Airlines A321 passenger jet on O'Hare's 4R runway. During these overruns, which occurred at a runway with an EMAS, there were no passenger injuries and only minimal aircraft damage.

An EMAS is a passive system; no external energy source is required for system performance. A cementitious type material is used in the EMAS. An EMAS is

positioned within the runway safety area (RSA) set back from the runway threshold. The setback length protects the arrestor material from jet blast, prevents the arrestor bed from being an obstruction during an undershoot, and provides space to avoid aircraft intrusion during a low velocity overrun, Figure 1.1. The EMAS works to bring an aircraft to stoppage by developing drag forces on the landing gear through arrestor material – tire interaction. The EMAS drag forces significantly reduce an aircraft's stopping distance without damaging aircraft landing gear or inducing significant inertia force on the aircraft passengers. An EMAS is designed based on an airport's expected aircraft fleet and available runway end safety area. Preliminary EMAS design guides are available in the FAA Advisory Circular (AC) 150/5220-22A (Federal Aviation Administration, 2005) and were developed for DC-9, DC-10, B737-400, B757, B747, CRJ-200, G-III aircraft types. The design guides plot required EMAS length as a function of maximum runway exit speed for each aircraft type. Worse case conditions are assumed using zero reverse thrust and poor braking (friction coefficient = 0.25). The EMAS length in each plot includes a 75-ft pavement lead-in rigid ramp. Consequently, the EMAS arrestor material bed length is equal to the plot EMAS length minus 75-ft. Another EMAS length chart for preliminary design is available in FAA Order 5200.9 (Federal Aviation Administration, 2004). This chart is not aircraft specific, but instead provides EMAS material bed length as a function of maximum aircraft takeoff weight. These preliminary design guides provide EMAS length estimates; however, FAA AC 150/5220-22A requires that an EMAS be designed using a validated design method (Federal Aviation Administration, 2005).

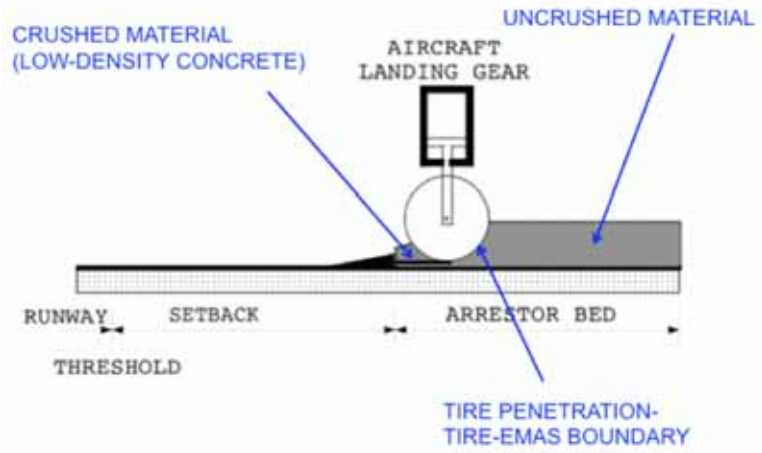

Figure 1.1. Aircraft Movement Through an EMAS

Figure 1.2 shows an installed EMAS at Adams Field in Little Rock, AR (Google Earth, 2009). The river in the picture is a natural barrier and prevents runway extension. The runway safety area includes a lead-in rigid ramp between the runway threshold and the arrestor bed. The ramp is sloped to improve tire entry performance into the arrestor bed material. EMAS sides and end are stepped to allow access to aircraft rescue and firefighting vehicles (ARFF), Figure 1.3.

Figure 1.2. Installed EMAS at Adams Field; Little Rock, AR

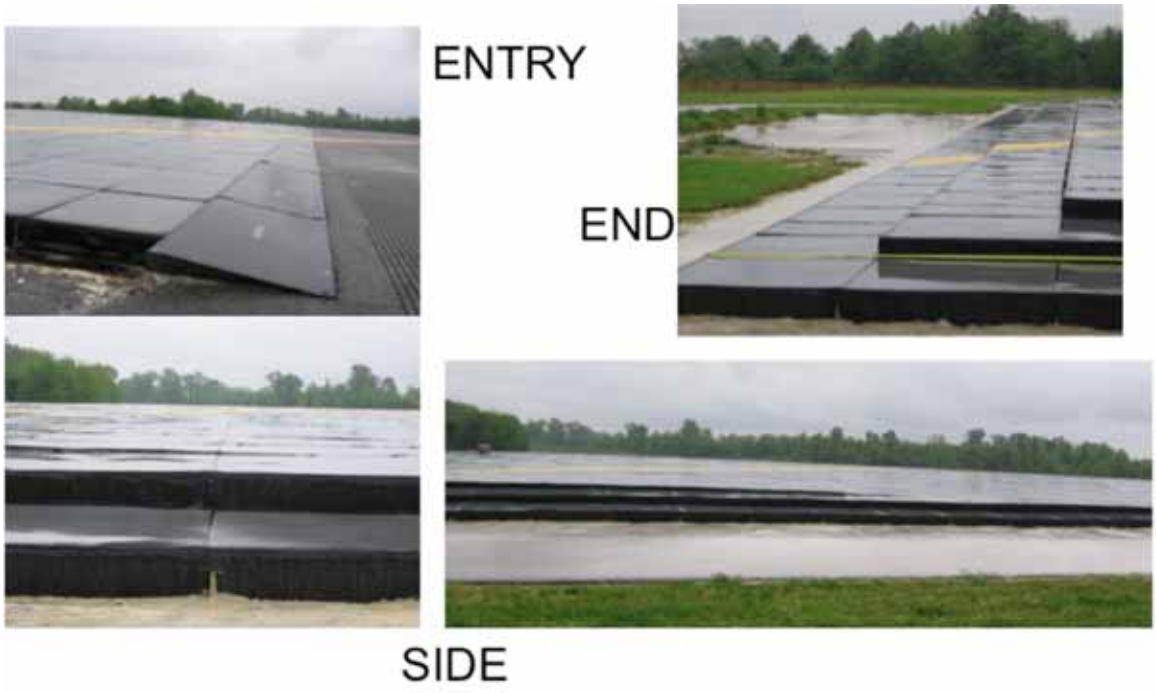

Figure 1.3. Adams Field EMAS Installation

Chapter 2
EMAS Design Requirements

EMAS design requirements are included in Advisory Circular 150/5220-22A, "Engineered Materials Arresting Systems (EMAS) for Aircraft Overruns" (Federal Aviation Administration, 2005). Fourteen design requirements are detailed in the Advisory Circular (AC): concept, location, design method, operation, width, base, entrance speed, aircraft evacuation, maintenance, undershoots, navigation aids, drainage, jet blast, and repair. A brief summary of each of the design requirement details is given in the following.

1. Concept: The purpose of an EMAS is to stop an aircraft during an overrun by exerting predictable drag forces on the aircraft landing gear. Passenger safety is paramount along with minimizing aircraft damage in the case of an overrun. For passenger safety, maximum aircraft deceleration is to be limited to an acceptable value. Because of the intrinsic characteristics of a low-density material, durability is a major design concern. An EMAS arrestor bed material should have a service life of 20 years.
2. Location. The EMAS is located at the runway end within the runway safety area (RSA). It is placed using the greatest permissible setback distance that space will allow to: avoid deterioration due to jet blast, obstructing an aircraft during an undershoot, and avoid aircraft intrusion during a low velocity overrun.
3. Design Method. The method used to design an EMAS is required to be a proven method that has been validated. An EMAS design is site specific and needs to consider the aircraft mix at the location. Design charts provided in AC 150/5220-22A are only to be used for preliminary design.
4. Operation. The EMAS is designed as a passive system. Consequently, no outside energy source is warranted.
5. Width. The EMAS full-thickness width is the same as the design runway width. EMAS steps used for emergency vehicle access occur outside the design runway width.

6. Base. The EMAS is supported by a paved surface. The paved surfaced is designed for EMAS weight, the critical aircraft in the event of an overrun, and aircraft rescue and fire fighting (ARFF) vehicles.
7. Entrance Speed. Based on historical data, the aircraft is assumed to enter the runway end safety area at 70 knots. Poor aircraft operation conditions are assumed so that the EMAS design is based on 0 aircraft reverse thrust and poor braking conditions equivalent to a 0.25 tire-pavement friction coefficient.
8. Aircraft Evacuation. Sloped sides or steps are provided along each arrestor side for aircraft rescue and fire fighting vehicle (ARFF) access during an overrun. The EMAS material is designed to support an aircraft rescue and fire-fighting vehicle (ARFF) in the event of an overrun. Limited EMAS material deformation is permissible during emergency operations; however, ARFF vehicle mobility is essential in the event of an emergency aircraft evacuation.
9. Maintenance Access. EMAS material must be capable of supporting pedestrian maintenance traffic with no material deformation.
10. Undershoots. The EMAS is designed and located in the RESA so as not to cause aircraft control problems when an aircraft lands short.
11. Navigation Aids. EMAS blocks used within the arrestor bed are positioned to accommodate runway navigational lighting.
12. Drainage. Proper drainage is to be provided to prevent any water accumulation.
13. Jet Blast. The EMAS is positioned in the RSA with a setback distance from the runway threshold to prevent material damage from jet blast.
14. Repair. In the event of an overrun, an EMAS is to be fully repaired within 45 days of an aircraft overrun.

Chapter 3
Full-Scale Testing

Full-scale testing was conducted at the Minneapolis-St. Paul International Airport comparing vehicle penetration on an installed EMAS. Each test vehicle was introduced into the EMAS at an entry velocity. The EMAS experienced only minor damage due to the weight of a sport utility vehicle (SUV), Figure 3.1. A second test was conducted using an ARFF, Figure 3.2. The heavier weight vehicle caused greater damage; however, the ARFF was still mobile within the arrestor bed. Similarly, a snowplow entering the EMAS at entry velocity showed significant material damage, but the snowplow was still mobile, Figure 3.3. During the mid 1990's the FAA conducted full-scale testing on an EMAS using a B727. In the last test conducted, the B727 entered the EMAS at 55 knots, Figure 3.4. The aircraft nose gear separated from the fuselage at 100-ft into the arrestor bed and stopped at 260-ft, 16-ft within the stopping distance predicted by a numerical model developed for the test. While in the EMAS, the B727 aircraft experienced semi-constant deceleration below 1g.

Figure 3.1. EMAS Material Deformation due to a SUV.

Figure 3.2. EMAS Material Deformation due to an ARFF

Figure 3.3. EMAS Material Deformation due to a Snowplow

Figure 3.4. FAA Full-Scale Testing using a B727 (FAA Tech Center Video, ftp://ftp.tc.faa.gov/aar410/RPD 148/Emasmpg.mpg**)**

Chapter 4
Numerical Analysis

4.1 Numerical Analysis Formulation

The FAA uses the ARRESTOR computer code to predict stopping distance of an aircraft moving through an EMAS. The FAA technical report by Cook et al. describes the ARRESTOR code (Cook et al., 1995). ARRESTOR is an extended work of the FITER1 computer code. FITER1 was initially developed by Cook and used to predict fighter plane movements on soft ground (Cook, 1985). The executable for ARRESTOR is available through the FAA. In an ARRESTOR analysis session, the user supplies information through user-friendly pop-up windows. Required user input includes: EMAS geometry, EMAS material properties, and limited aircraft properties. Because of the complexity of the required aircraft properties needed for a stopping distance analysis, the ARRESTOR code is linked to data files that include aircraft parameters. Consequently, the user is responsible for inputting only the aircraft type, aircraft weight, and aircraft center-of-gravity location in terms of percent mean aerodynamic chord (% MAC). Only three aircraft types are available for an ARRESTOR analysis: B707, B727, and B747. In order to analyze more up-to-date aircraft types, a new computer code, SGAS (soft ground arrestor system), was developed during this study. Although user-friendly input windows are not included in the new SGAS code, the input format has been greatly simplified by requiring only the aircraft parameters directly related to aircraft movement through an EMAS. An overview of input and output required for the two computer codes, ARRESTOR and SGAS, is shown in Figure 4.1.

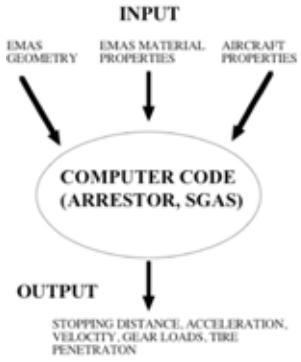

Figure 4.1. Numerical Analysis Input-Output Format.

Aircraft motion within the runway safety area is calculated applying three governing equations: force equilibrium in the aircraft motion direction, moment equilibrium about the aircraft pitch axis, and force equilibrium along the strut axis at each landing gear strut. The analysis is conducted in the time domain at incremental time steps. The numerical analysis continues until a preset maximum time or when the aircraft velocity approaches a minimal value close to zero. Motion at each time step is calculated using the aircraft position at the end of the previous time step as an initial value for the subsequent time step. Consequently, force equilibrium in the direction of the aircraft is used to calculate the aircraft acceleration for the start of the following time step. At each incremental time step, the horizontal acceleration, $\ddot{x}$, in the direction of the aircraft is controlled by:

$$m\ddot{x} = Fdrag_{ng} + Fdrag_{mg,wing} + Fdrag_{mg,body} \tag{4.1}$$

In equation (4.1), m is the total aircraft mass, the drag force acting at the nose landing gear strut is $Fdrag_{ng}$, and $Fdrag_{mg,wing}$ is the summation of the drag forces acting at the wing main landing gear struts. $Fdrag_{mg,body}$ is included in equation (4.1) for aircraft that have body landing gear and represents the summation of the drag forces acting at the body main landing gear struts to oppose aircraft horizontal motion. Drag forces oppose motion and therefore will have negative values in equation (4.1). Since the considered aircraft motion is within the runway safety area, low velocity is assumed and aerodynamic drag forces are neglected in equation (4.1). Aircraft distance traveled, x, at time t_i is calculated through time integration of the aircraft acceleration over the time step and adding this incremental displacement to the aircraft's x location at time, t_{i-1}

Aircraft pitch angle and landing gear stroke change incrementally as a function of time as the aircraft moves through the arrestor bed. Consequently, these changes produce changes to the location of the aircraft center of gravity and its position relative to the pavement. By considering external forces acting on the aircraft, moment equilibrium about the aircraft center of gravity pitch axis is used to calculate the aircraft angular acceleration:

$$I\ddot{\theta}_{pitch} = (F\,arrestor_{arrestor,\,ng} - W\,unsprung_{ng}) * x_{ng} + (F\,drag_{ng} * z_{ng})$$
$$- (F\,arrestor_{mg,\,wing} - W\,unsprung_{mg,\,wing}) * x_{mg,\,wing} + (F\,drag_{mg,\,wing} * z_{mg,\,wing})$$
$$- (F\,arrestor_{mg,\,body} - W\,unsprung_{mg,\,body}) * x_{mg,\,body} + (F\,drag_{mg,\,body} * z_{mg,\,body})$$

(4.2)

In equation (4.2), the aircraft mass moment of inertia about the pitch axis is I and $\ddot{\theta}_{pitch}$ is the aircraft angular acceleration about the pitch axis. At each landing gear strut, Farrestor vertical forces act at the arrestor-tire boundary, Fdrag horizontal drag forces act on the tire, and Wunsprung is the landing gear strut weight. The horizontal and vertical distances between the aircraft center of gravity and undeformed tire base at each strut are x and z, respectively. $\ddot{\theta}_{pitch}$ is integrated over each time step increment to find θ_{pitch}. θ_{pitch} is positive for aircraft nose up rotation about the pitch axis from the aircraft's original row axis.

Stroke at each landing gear, $s_{gear\,i}$, is calculated integrating $\ddot{s}_{gear\,i}$ over each incremental time step. Vertical force equilibrium is applied at each landing gear strut to determine the strut's stroke acceleration:

$$m_{gear\,i}\ddot{s}_{gear\,i} = F\,arrestor_{gear\,i} - W\,unsprung_{gear\,i} + F\,strut_{gear\,i}$$

(4.3)

In equation (4.3), the unsprung landing gear mass at gear i is $m_{gear\ i}$. Farrestor $_{gear\ i}$ is the arrestor material vertical force at gear i and $Fstrut_{gear\ i}$ is the strut force at gear i.

For each incremental time step, x, θ_{pitch}, and, $s_{gear\,i}$ initial values are set to the previous time step calculated end values. An SGAS output file records aircraft behavior (translation, velocity, deceleration, landing gear forces, and wheel axle height) and arrestor material behavior (crushed material thickness) at equal time increments. The output included in the SGAS output file is formatted to copy and paste into an Excel file for graphical SGAS data presentation. Two Excel file formats were developed during

this study. One Excel file is for aircraft with only wing main landing gear. A second Excel file was developed for aircraft with wing and body main landing gear.

4.2 Tire-Arrestor Material Interaction

The tire-soil numerical model discussed in the reference by Phillips and Cook was used as a basis for the tire-arrestor material numerical model used in SGAS (Phillips & Cook, 1983). In the Phillips and Cook model, non-linear springs represent the tire stiffness and soil is modeled as a visco-elastic material. The model assumes a Maxwell material, spring and damper in series, for the soil. Conversely, in this study the Maxwell material model used for soil is replaced by sliders, springs with no rebound. Consequently, the arrestor material behavior is fully plastic with zero rebound. The tire-EMAS interaction numerical model used for a dual wheel configuration and dual tandem configuration are shown in Figure 4.2.

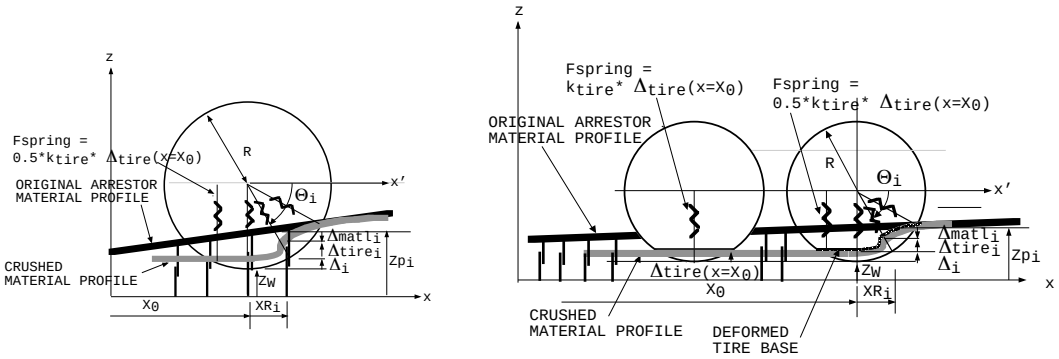

a) Dual Wheel Landing Gear Configuration b) Dual Tandem Landing Gear Configuration

```
X0 =  threshold - wheel center horiz. dist.
XRi=  wheel center - SPRINGi horiz. dist.
ZW=   undeformed tire base height @ tire center
Θi= angle from horiz. to SPRINGi
Zpi = arrestor material height @ SPRINGi
Δi= dist. from base of undeformed tire to
undeformed tire @ SPRINGi
Δmatli = arrestor material deformation at
            SPRINGi(+down)
Δtirei = tire deformation @ SPRINGi(+up)
ktire =  tire stiffness
```

Figure 4.2. Tire-EMAS Interaction Model

For a SGAS analysis, arrestor material behavior is entered at incremental strain values as stress as a function of strain. Tire behavior is calculated modeling the tire as a set of radial nonlinear springs, as shown in Figure 4.2. Each spring in the front bottom quarter of the tire is assumed to have the same radial stiffness behavior. Since the arrestor material is a crushable material, the material behind the tire axle, $x_{0,}$ has already been crushed. This region behind the tire axle is assumed to have a constant thickness, the same thickness as at the tire axle. Consequently, a linear spring equal to half the tire stiffness is used to model the back half of the tire. Spring constants used to model the tire as a set of springs are developed from tire manufacturer load-deflection diagrams, which are available through tire manufacturers. In SGAS, A trial-and-error approach is used to equate the vertical tire force component with the arrestor material vertical force. To insure tire-EMAS contact, equation (4.4) must be satisfied:

$$Z_w + \Delta_i + \Delta tire_i = Zp_i - \Delta matl_i \tag{4.4}$$

where the variables in Equation (4.4) are defined in Figure 4.2. Each spring's horizontal force component contributes to resisting the total drag force induced by the arrestor bed. Each spring's vertical force component balances the arrestor material's vertical force. Interaction between the tire face and arrestor material is limited to a range between the first spring location, $\theta_{i=1}$, and $\theta_i = 90.0^\circ$ in Figure 4.2.

4.3 FAA ARRESTOR Code Description

In the following, a brief description is given of the FAA ARRESTOR computer code and its usage. The reference by Cook et al. gives a more detailed description (Cook et al., 1995). An overview of the ARRESTOR input and output is shown in Figure 4.3.

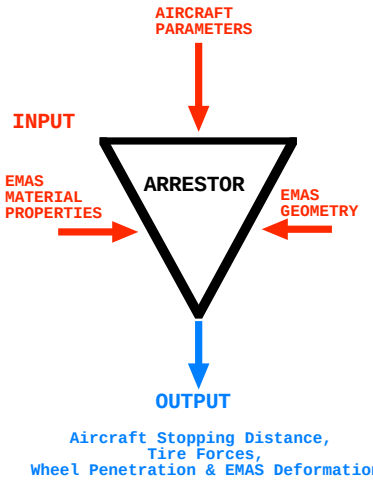

Figure 4.3. FAA ARRESTOR Input – Output

Detailed aircraft parameters are supplied to the ARRESTOR code through three linked data files. Each data file includes aircraft parameters such that when the user inputs the aircraft type, the specific aircraft parameters are included in the analysis. The ARRESTOR code is capable of analyzing three aircraft types: B707, B727, and B747. Two Excel data files, B707 / B727 and B747, were developed in this study to present the ARRESTOR output in graphical format to better visualize the ARRESTOR numerical output.

4.4 FAA ARRESTOR Code Input

An ARRESTOR analysis begins by the user executing the ARRESTOR code. A pop-up window appears defining user options, Figure 4.4.

Figure 4.4. ARRESTOR Code Menu

The “Define Materials”, “Design Arrestor”, and “Select Aircraft” buttons are used for user input. After information has been supplied for each of the three input categories, the user selects “Start Calculation” for the ARRESTOR analysis.

Define Materials

The “Define Materials” button on the ARRESTOR Menu activates a new pop-up window for the user to numerically describe the arrestor material stress-strain behavior, Figure 4.5. Up to two types of arrestor bed materials are allowed to be considered for the EMAS bed, Press1 and Press 2. Press1 corresponds to the arrestor bed material closest to the EMAS entry. If a second material is used, it is denoted as Press 2. The user supplies the material stress-strain behavior at set ARRESTOR strain values (0.2, 0.3, 0.4, …). Stress can also be entered in the light blue boxes to describe material rebound behavior if it exists. Typically, EMAS material has only minimal rebound. Figure 4.5 shows the stress-strain behavior of a typical low-density concrete. The figure depicts the behavior of a crushable material. At a minimum stress, the material begins to deform and experiences large increases in strain, crushing, without additional stress. After the “necking region”, approximately 60% strain, additional stress is required to cause additional strain. At high strains, above 80% strain, a significant stress increase is required to cause additional strain so that the plot becomes asymptotic.

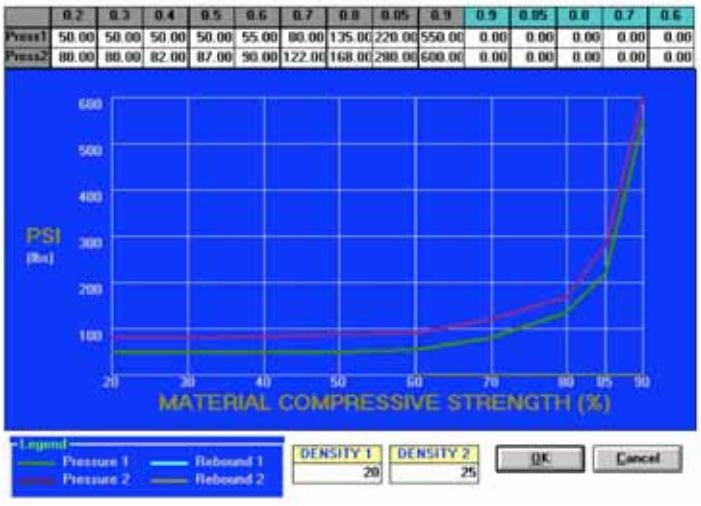

Figure 4.5. EMAS Material Behavior Pop-Up Window.

DESIGN ARRESTOR

The user inputs the EMAS configuration by selecting the "Design Arrestor" button on the ARRESTOR menu pop-up window. After selecting "Design Arrestor" a new pop-up window is activated allowing the user to specify height and length dimensions of the rigid lead-in ramp, and two arrestor bed sections, Section 1 and Section 2, Figure 4.6. Material properties for the two sections correspond to Press1 and Press2 of Figure 4.5. For the lead-in ramp, the user supplies the distance from the threshold to the start of the rigid ramp and the ramp slope. For each of the two arrestor bed sections, the user inputs the starting point of the arrestor bed section, initial bed height, the maximum section bed height, the slope between the initial and maximum arrestor bed height, and the distance from threshold that the section ends.

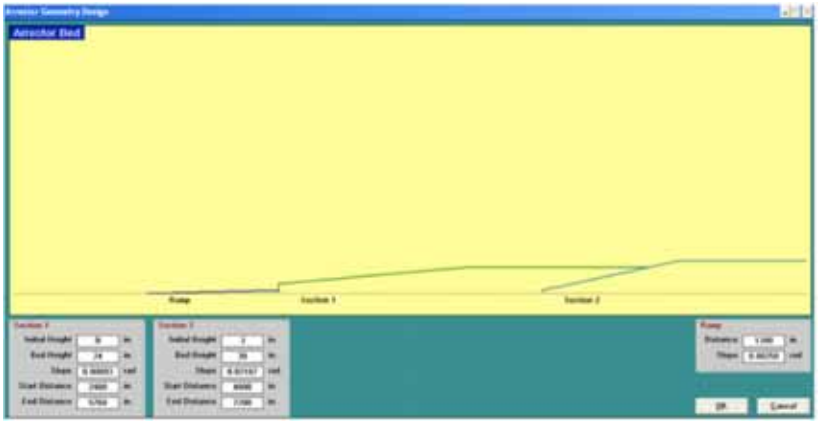

Figure 4.6 EMAS Geometry Pop-Up Window.

Select Aircraft

The aircraft properties required to be entered for an ARRESTOR analysis is simplified using existing data files that include aircraft properties for three specific aircraft types: B707, B727, and B747. After activating the "Aircraft Properties" button on the ARRESTOR pop-up menu, a new pop-up window appears to enter data relevant to the specific aircraft to be analyzed, Figure 4.7. In the new pop-up window, the user selects the aircraft type, gross weight, mass moment of inertia, and aircraft center-of-gravity. The user supplies additional information to describe the initial aircraft velocity as the aircraft enters the runway safety area, the applied fraction of reverse thrust, and

wheel-pavement friction. Main landing gear braking is incorporated into the analysis by the user entering an increased friction value.

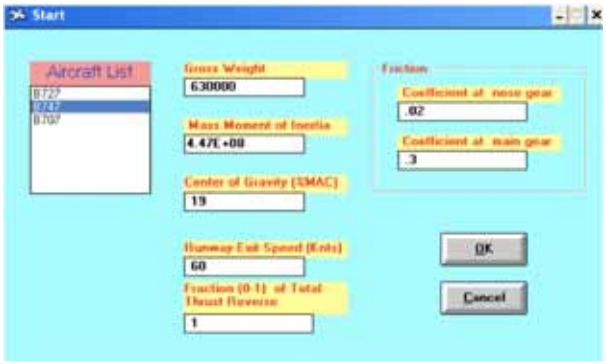

Figure 4.7. ARRESTOR Select Aircraft Pop-Up Window.

4.5 FAA ARRESTOR Code Output

After entering the input required for an ARRESTOR analysis, an ARRESTOR analysis is performed using the "Start Calculation" button on the ARRESTOR menu pop-up window, Figure 4.4. An ARRESTOR analysis creates a single output file, Plt1, for a B707 or B727 aircraft analysis. Conversely, because of its characteristic B747 landing gear configuration, two files, Plt1 and Plt2, are created in a B747 analysis. Excel files were developed during this study to present the ARRESTOR data output files in graphical format. To show the output as plots, the user copies the Plt data into the corresponding Excel file data window. Plots are then automatically generated.

4.6 SGAS Code Input

Two files are required to conduct an aircraft stopping distance analysis using SGAS. One file is the run file. It includes the number of problems to be conducted, and the input and output file names. An example of a SGAS run file is included in the Appendix A. The first line of the run file includes the number of problems to be performed. Subsequent lines include the name of the input file, which is supplied by the user, and the name of the output data file developed during an SGAS analysis. A comment card can be included on any line of the run file by typing an exclamation mark

(!) in the first column. A sample input file for a B747 aircraft is also included in the Appendix A. Similar to the SGAS run file, a comment line can be included on any line of the input file. The comment cards in the sample SGAS input file are included to describe the data on each line.

4.7 SGAS Code Output

The user performs a SGAS analysis by executing SGAS and responding to the code's query for the name of the SGAS run file. After the SGAS analysis is completed, output can be copied and pasted in Excel files developed especially for the SGAS output to convert SGAS output data into plot format. Two Excel files, wing gear (WG-SGAS.xls), and wing gear & body gear (WG&BG-SGAS.xls) for the B747 aircraft, were developed during this study in order to present SGAS output in plot format.

Chapter 5
Aircraft Strut Behavior

5.1 Oleo-Pneumatic Strut

The plane's motion as it moves through the arrestor bed is controlled by the characteristics of the aircraft and arrestor bed material. Aircraft deceleration is controlled by drag through tire – arrestor material interaction. Load distribution between the nose landing gear strut and main landing gear struts is a function of aircraft strut behavior. The axial force developed in the landing gear strut is from a combined effect of pneumatic strut force and hydraulic strut force. A typical aircraft strut is shown in Figure 5.1. The typical aircraft strut, oleo-pneumatic strut, consists of an outer cylinder and an inner cylinder. The inner cylinder slides within the outer cylinder. The inner cylinder is filled with hydraulic fluid while the outer cylinder contains air. As the inner cylinder moves, hydraulic fluid flows through the orifice, a small opening, which results in energy dissipation. A variable diameter pin connected to the inner chamber slides through the orifice and controls the effective orifice area available for fluid flow. Consequently, the air in the outer cylinder provides for strut stiffness, load as a function of stroke, while the hydraulic fluid serves as a damper, load as a function of stroke velocity (Curry, 1988).

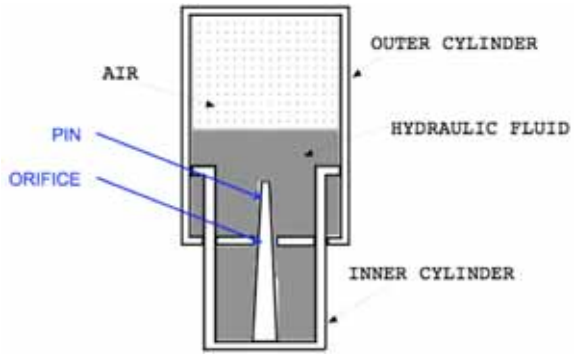

Figure 5.1. Oleo-Pneumatic Strut

5.2 Pneumatic Strut Force

The force within the outer cylinder is controlled by air pressure. Figure 5.2 illustrates the condition within the outer cylinder. Two air chamber conditions are shown

in Figure 5.2, fully extended at minimum air pressure (FE), and secondly, at an arbitrary stroke distance (s).

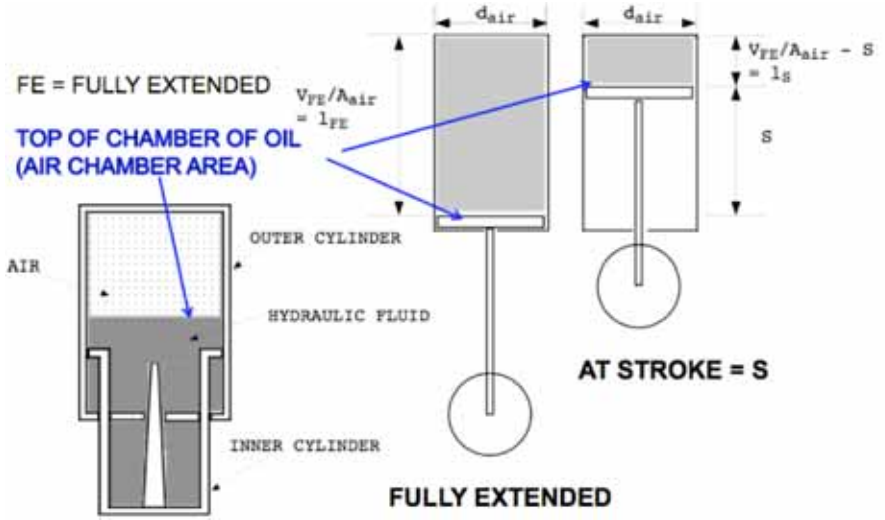

Figure 5.2. Pneumatic Strut Force

The pneumatic strut force is calculated using the idea gas law. For low stroke velocity, representative of normal aircraft land movements, isothermal compression and expansion is assumed and the ideal gas law can be written as:

$$\underbrace{(p_{gage}(s) + p_{atm})}_{p_{absolute}(s)} \cdot l_s \cdot A_{air} = constant \tag{5.1}$$

$p_{gage}(s)$ is the gage pressure at stroke s, p_{atm} is the atmospheric pressure, 14.7 psi (101.3 kPa). The atmospheric pressure converts gage pressure, $p_{gage}(s)$ to absolute pressure, $p_{absolute}(s)$, at stroke s. A_{air} is the outer cylinder cross-section area and l_s is the height of the confined air at stroke s. For isothermal compression/expansion, the pressure-volume product is a constant. Therefore, the pressure-volume product at any stroke, s, is equal to the pressure-volume product at the strut's fully extended stroke condition:

$$(p_{gage}(FE) + p_{atm}) \cdot V_{FE} = (p_{gage}(s) + p_{atm}) \cdot l_s \cdot A_{air} \tag{5.2}$$

and equation (5.2) can then be solved for the gage pressure at any stroke, s:

$$p_{gage}(s) = \frac{(p_{gage}(FE) + p_{atm}) \cdot V_{FE}}{l_s \cdot A_{air}} - p_{atm} \tag{5.3}$$

The pneumatic force in the outer cylinder is attained using equation (5.3) and the outer chamber cross-section area:

$$F_{air}(s) = \frac{p_{gage}(FE) \cdot V_{FE}}{\frac{V_{FE}}{A_{air}} - S} \tag{5.4}$$

Equations (5.2), (5.3), and (5.4) are written in terms of V_{FE}, air chamber volume at fully-extended stroke. The pressure-volume product at fully extended stroke is also equal to the pressure-volume product when the air chamber is fully compressed, FC:

$$(p_{gage}(FE) + p_{atm})V_{FE} = (p_{gage}(FC) + p_{atm})V_{FC} \tag{5.5}$$

The air chamber volume difference between fully compressed and fully extended, ΔV_{max}, equals the displaced air volume as the piston moves from minimum pressure at its fully extended position to maximum pressure at the strut's fully compressed position:

$$V_{FC} = V_{FE} - \Delta V_{\max} \tag{5.6}$$

where

$$\Delta V_{MAX} = S_{MAX} * A_{air}$$

To solve for V_{FE}, substitute equation (5.6) into equation (5.5):

$$V_{FE} = \frac{(p_{gage}(FC) + p_{atm})}{(p_{gage}(FE) + p_{atm})}(V_{FE} - \Delta V_{\max})$$

(5.7)

and then solve for V_{FE}

$$V_{FE} = \frac{p_{abs}(FC) * \Delta V_{MAX}}{p_{gage}(FC) - p_{gage}(FE)}$$

(5.8)

Equation (5.8) determines maximum air volume within the outer chamber when the strut is fully extended in terms of pressure and maximum stroke.

Volume at any stroke is then determined using:

$$V(s) = \frac{p_{abs}(FE)}{p_{abs}(s)} V_{FE}$$

(5.9)

The previous formulation assumes isothermal behavior and therefore low stroke velocity. Conversely, at high stroke velocity, a more accurate assumption is polytropic compression behavior where:

$$(p_{gage}(s) + p_{atm})V(s)^{1.35} = constant$$

(5.10)

Typically, during normal aircraft ground movements, semi-static conditions exist and the strut stroke will be less than the static extension stroke, S_{SE} . Conversely, during dynamic conditions (aircraft landing, impact, and bumps), the strut stroke will be greater than static stroke. Consequently, for $S < S_{SE}$, isothermal compression is assumed ($p_{absolute}$ V = constant); however, for $S > S_{SE}$, polytropic compression is assumed ($p_{absolute}$ $V^{1.35}$ = constant). Since stroke at the aircraft's static position represents a transition point between semi-static and dynamic stroke behavior, the polytropic constant is established

using the pressure and volume at strut static extension, SE. Considering both semi-static and dynamic stroke behavior, for stroke less than static extension stroke,
equation (5.3) is written as:

$$p_{gage}(S) = \frac{p_{abs}(SE) * V_{SE}}{V(S)} - p_{atm}$$

(5.11)

Conversely, for stroke greater than static extension stroke, polytropic compression behavior, equation (5.3) is rewritten as:

$$p_{gage}(s) = \frac{p_{abs}(SE) * V_{SE}^{1.35}}{V(s)} - p_{atm}$$

(5.12)

5.3 Hydraulic Strut Force

Whereas the pneumatic force is a function of strut stroke, the hydraulic strut force is dependent on stroke velocity. As the hydraulic fluid flows through the orifice in Figure 5.3, energy is dissipated. A pin within the inner cylinder that slides through the orifice controls the effective orifice diameter. As stroke increases, the effective orifice diameter decreases.

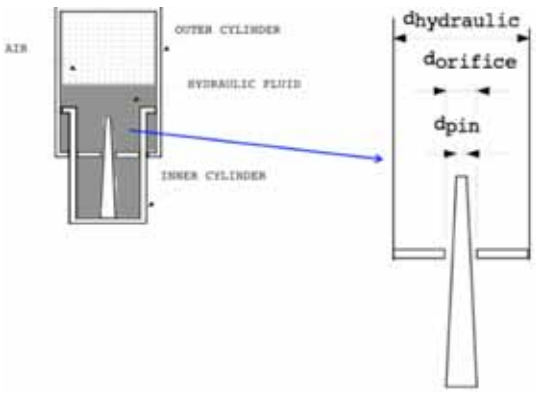

Figure 5.3. Hydraulic Strut Force

The hydraulic force is a function of strut velocity and is equal to:

$$F_{hydraulic} = \frac{\rho_{hydraulic} A_{hydraulic}^3 \frac{ds}{dt}\left|\frac{ds}{dt}\right|}{2(C_d A_{eff\ orif})^2} \tag{5.13}$$

$\rho_{hydraulic}$ is the hydraulic fluid density (0.000077 #/(in/sec^2)/in^3), $A_{hydraulic}$ is the oil chamber area, ds/dt is the stroke velocity, C_d is the orifice coefficient and taken equal to 0.9 (Gerardi, 1977). $A_{eff\ orif}$ is the orifice cross sectional area that the oil flows through:

$$A_{eff\ orif} = \frac{\pi d_{orifice}^2}{4} - \frac{\pi d_{pin}^2}{4} = A_{orifice} - A_{pin} \tag{5.14}$$

$F_{hydraulic}$ acts to oppose stroke. Consequently, $F_{hydraulic}$ increases the strut force for positive stroke velocity and decreases the strut force in the case of negative stroke velocity.

For increasing stroke: $\frac{ds}{dt} \geq 0; \quad F_{hydraulic} \geq 0$

For decreasing stroke: $\frac{ds}{dt} \leq 0; \quad F_{hydraulic} \leq 0$

(5.15)

Equation (5.13) can be simplified and rewritten as:

$$F_{hydraulic} = C * \frac{ds}{dt}\left|\frac{ds}{dt}\right| \tag{5.16}$$

where C is the damping force factor and equal to:

$$C = \frac{\rho_{hydraulic} A_{hydraulic}^3}{2(C_d A_{eff\ orif})^2} \tag{5.17}$$

The total strut force acting on the landing gear wheel and on the aircraft is the combined effect of the force in the air chamber and in the hydraulic fluid:

$$F_{strut} = F_{air} + F_{hydraulic} \tag{5.18}$$

Chapter 6
Methodology to Develop Approximate Values for Aircraft Parameters

6.1 Available Information on Aircraft Parameters

For the B737-900ER, B747-400ER, B757-300, and B767-400ER aircraft types considered in this study, maximum gross takeoff weight, dimensions, and tire size are available in the Boeing Airplane Characteristics for Airport Planning Guides (Boeing Co. 1985, 2002a, 2002b, 2005a, & 2005b). Equivalent spring stiffness for the tire model is derived using tire stiffness graphs available through tire manufacturers such as Goodrich, Goodyear, or Michelin. Conversely, information describing aircraft characteristics related to the strut and pitch axis moment of inertia are limited. Therefore, an approximate approach was derived in this study to attain these values. Load-stroke behavior, strut damping, unsprung weights, and moment of inertia about the aircraft pitch axis are available for older aircraft in a reference by Gerardi (Gerardi, 1977). The Gerardi reference includes information on DC-9-41, B727-200, B707-320C, DC-10-10, and B747-200 aircraft types. Relevant information from the Gerardi reference is summarized in Table 6.1. The characteristics of the aircraft investigated in this study were derived extrapolating aircraft data described in the Gerardi reference. Investigated aircraft were grouped with aircraft described in the Gerardi reference based on aircraft gross weight.

Table 6.1. Aircraft Parameters (Gerardi, 1977)

AIRCRAFT TYPE		DC-9-41	B727-200	B707-320C	DC-10-10	B747-200
GROSS WEIGHT	lb	114,000	160,000	306,000	440,000	630,000
	N	507,300	712,000	1,361,700	1,958,000	2,803,500
MOM. of INERTIA	lb in sec^2	21,540,000	62,800,000	84,700,000	211,600,000	488,000,000
	kg*m^2	2,435,825	7,101,662	9,578,197	23,928,531	55,184,892
DIMENSIONS						
NG (# TIRES)		2	2	2	2	2
MG CONFIG		DUAL	DUAL	DUAL TANDEM	DUAL TANDEM	DUAL TANDEM
NG-CG DIST	ft (m)	54.37 (16.58)	59.79 (18.23)	56.50 (17.23)	66.57 (20.30)	76.29 (23.26)
CG-MG1 DIST	ft (m)	2.03 (0.62)	3.23 (0.98)	2.50 (0.76)	6.08 (1.85)	2.67 (0.81)
CG-MG2 DIST	ft (m)					12.75 (3.89)
LOAD / STRUT						
NG MAX VERT LOAD	lb (N)	17220 (76630)	25600 (113920)	51770 (230400)	84959 (378100)	135700 (603900)
MG MAX VERT LOAD	lb (N)	53817 (239500)	87800 (390710)	157000 (698700)	213680 (950900)	183800 (817910)
NG UNSPRUNG WT.	lb (N)	164 (730)	495 (2203)	432 (1922)	652 (2901)	1750 (7790)
MG UNSPRUNG WT.	lb (N)	1074 (4779)	1363 (6065)	1659 (7383)	5104 (22713)	3900 (17355)
MAX STROKE						
NG	in (mm)	15.3 (389)	12.1 (307)	17.1 (434)	17.2 (437)	25.2 (640)
MG	in (mm)	17.8 (452)	14.0 (356)	23.2 (589)	24.5 (622)	28.8 (732)
DAMPING COEFF.						
NG	lb/(in/s)^2	0.29	3.33	3.14	37.25	9.90
NG	N/(mm/s)^2	0.0020	0.0230	0.0217	0.2570	0.0683
MG	lb/(in/s)^2	0.51	3.81	17.34	41.33	9.13
MG	N/(mm/s)^2	0.0035	0.0263	0.1196	0.2851	0.0630

6.2 Mass Moment of Inertia about the Pitch Axis, I_{yy}

To determine an approximate value for the mass moment of inertia about the pitch axis, I_{yy}, the mass moment of inertia was calculated replacing the aircraft with a rod of the same total length and with the aircraft weight uniformly distributed along its length, Figure 6.1. The mass moment of inertia for a rod with a uniformly distributed mass is:

$$I_{yy}(calc) = \int r^2 dm = \int r^2 \frac{w}{g} dr = \frac{W}{gl} \int r^2 dr = \frac{W}{3gl}(x_1^3 + x_2^3) \tag{6.1}$$

Where g is gravity acceleration and the other variables in equation (6.1) are defined in Figure 6.1.

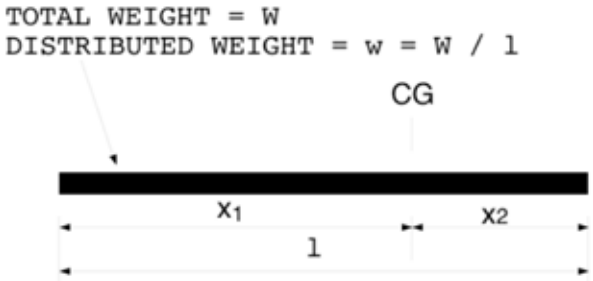

Figure 6.1. Mass Moment of Inertia of a Rod.

The calculated I_{yy} value using equation (6.1) was compared with the I_{yy} value given in the Gerardi reference to develop a conversion factor between the equation (6.1) rod value and the Gerardi reference aircraft value, Table 6.2. For the five aircraft types considered in the Gerardi reference, the conversion factor range was between 0.42 and 0.64. Upon review, a 0.45 conversion factor was selected for the aircraft in this study. Consequently, the values listed in Table 6.2 as I_{yy} (modified) were used as input to the SGAS computer code.

Table 6.2. Mass Moment of Inertia for Study Aircraft

AIRCRAFT TYPE	GW (#)	TOTAL LENGTH (ft)	X (NOSE-MG) (ft)	Iyy (calc) (#-in-s2)	Iyy (given) (#-in-s2)	CORRECTION FACTOR
DC-9-41	114000	113.3	63.7	47,558,959	21,540,000	0.45
B727-200	160000	136.2	78.33	98,416,272	62,800,001	0.64
B707-320C	306000	145.5	76.42	202,719,078	84,700,000	0.42
DC-10-10	440000	170.5	100.29	434,324,672	211,600,000	0.49
B747-200	630000	225.17	109.42	994,338,305	488,000,000	0.49
CORRECTION FACTOR =		0.45				
						Iyy (modified) (#-in-s2)
B737-900ER	171000	133.42	69.75	95,121,647		42,804,741
B747-400ER	910000	225.17	109.42	1,436,266,441		646,319,898
B757-300	270000	178.58	92.67	268,557,003		120,850,651
B767-400ER	450000	197.13	100.75	543,878,491		244,745,321

6.3 Unsprung Strut Weight

The ratio between unsprung weight and maximum gear vertical load was found to be fairly constant for the five aircraft types included in the Gerardi reference. At the nose gear strut, the ratio between the unsprung weight and maximum vertical load at the nose gear was approximately 0.01. Conversely, at the main landing gear, this ratio was approximately 0.02, Table 6.3. These ratios were then used to calculate approximate unsprung loads for the study aircraft as shown, Table 6.3.

Table 6.3 Aircraft Unsprung Weights

AIRCRAFT	DC-9-41	B727-200	B707-320C	DC-10-10	B747-200
UNSPRUNG WT (lb)					
NOSE GEAR	164	495	432	651.9	1750
MAIN LANDING	1074	1363	1659	5104.24	3900
MAX VERT LOAD (lb)					
NG (BREAKING)	17220	25600	51770	84959	135700
MG (AFT)	53817	87800	157000	213680	183800
NG WT. RATIO	0.010	0.019	0.008	0.008	0.013
MG WT. RATIO	0.020	0.016	0.011	0.024	0.021
	approximate ng wt ratio @ 0.01				
	approximate mg wt ratio @ 0.02				
AIRCRAFT	B737-900ER	B747-400ER	B757-300	B767-400ER	
GROSS WT. (lb)	171000	910000	270000	450000	
MAX VERT LOAD					
NG (BREAKING) (lb)	24810	122400	42800	59650	
MG (AFT) (lb)	88993	213600	125500	211850	
NG UNSPR. WT. RATIO	0.010	0.010	0.010	0.010	
MG UNSPR. WT. RATIO	0.020	0.020	0.020	0.020	
UNSPRUNG WT					
NOSE GEAR (lb)	248	1224	428	597	
NOSE GEAR (N)	1104	5447	1905	2654	
MAIN LANDING (lb)	1780	4272	2510	4237	
MAIN LANDING (N)	7920	19010	11170	18855	

6.4 Maximum Strut Stroke

For maximum stroke, the study aircraft were categorized with the Gerardi aircraft based on total gross weight, Table 6.4. Study aircraft were assigned a maximum stroke value for the nose and main landing gear similar to the corresponding Gerardi aircraft stroke value, Table 6.4.

Table 6.4. Maximum Aircraft Strut Stroke

	A	B	C	D	E
AIRCRAFT	DC-9-41	B727-200	B707-320C	DC-10-10	B747-200
GROSS WT. (lb)	114000	184800	333600	430000	775000
MAX VERT LOAD (lb)					
NG (BRAKING)	17220	25600	51770	84959	135700
STROKE (in)	15.3	12.1	17.1	17.2	25.2
STROKE (mm)	389	307	434	437	640
MAX VERT LOAD					
MG (AFT)	53817	87800	157000	213680	183800
STROKE (in)	17.8	14	23.2	24.5	28.8
STROKE (mm)	452	356	589	622	732
	B737-900ER	B747-400ER	B757-300	B767-400ER	
similar aircraft WT	(B)	(E)	(B)	(D)	
GROSS WT. (lb)	171000	910000	270000	450000	
MAX VERT LOAD (lb)					
NG (BRAKING)	24810	122400	42800	59650	
MG (AFT)	88993	213600	125500	211850	
NG STROKE (in)	12	25	12	17	
NG STROKE (mm)	305	635	305	432	
MG STROKE (in)	14	30	14	24	
MG STROKE (mm)	356	762	356	610	

6.5 Pneumatic Strut Force

A relationship for load-stroke behavior was developed using an approach described in the reference by Curry for ole-pneumatic shock absorber design (Curry, 1988). The approach considers strut behavior at three stroke positions: fully extended (FE), static extension (SE), and fully compressed (FC), Figure 6.2. The three stroke positions are set assuming that the air pressure at the strut's fully extended position (FE) is 25% of the static extension (SE) air pressure and the air pressure at the fully compressed position (FC) is triple that of the static extension (SE) air pressure. Air pressure at static extension is assumed at 1500 psi. Consequently, air pressure at fully extended stroke (FE) and fully compressed stroke (FC) are 375 psi and 4500 psi, respectively:

p_{gage} (SE) = 1500 psi (10335 kPa)
p_{gage} (SE) / p_{gage} (FE) = 4.0
p_{gage} (FE) = 375 psi (2583 kPa)
p_{gage} (FC) / p_{gage} (SE) = 3.0
p_{gage} (FC) = 4500 psi (31000 kPa)

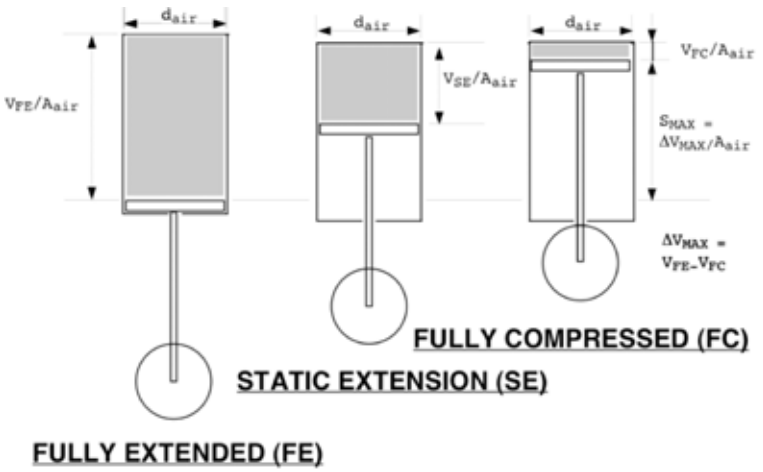

Figure 6.2. Stroke Positions used to Develop Stroke-Load Behavior

Stroke – Load Behavior Assuming Isothermal Conditions

The air chamber cross-section area, piston area, is calculated assuming maximum vertical strut load and pressure at SE stroke equal to 1500 psi:

$$Piston\ Area = A_{air} = \frac{V(static\ strut\ load)}{p_{gage}(SE)} \tag{6.2}$$

The equations described in section 5.2, Pneumatic Strut Force, are then used to develop a load-stroke behavior diagram assuming isothermal compression below SE stroke and polytropic compression above SE stroke. The load-stroke behavior of a B727-200 using the approach described in this section is shown in Figure 6.3. From the figure, load increases at a greater rate beyond SE stroke.

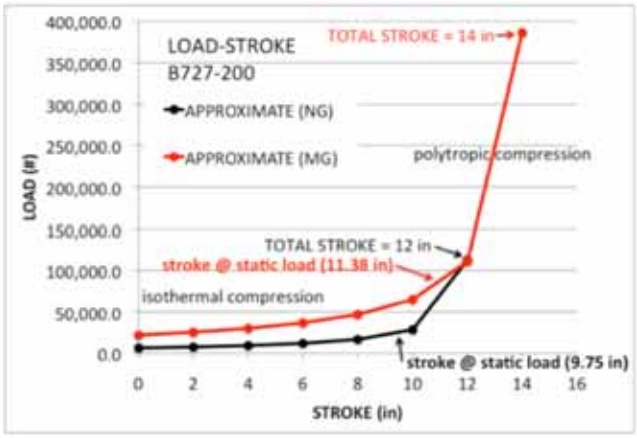

Figure 6.3. B727 Approximate Load-Stroke Behavior

A comparison is made in Figure 6.4 between the approximate approach and actual load-stroke behavior to show the accuracy of implementing the approximate load-stroke behavior approach. The actual load-stroke behavior in Figure 6.4 was developed using strut characteristics included in the Gerardi reference for the B727-200 aircraft (Gerardi, 1977). A comparison between the two methods shows that the approximate approach develops a load-stroke curve representative of the actual behavior developed using the more accurate Gerardi data.

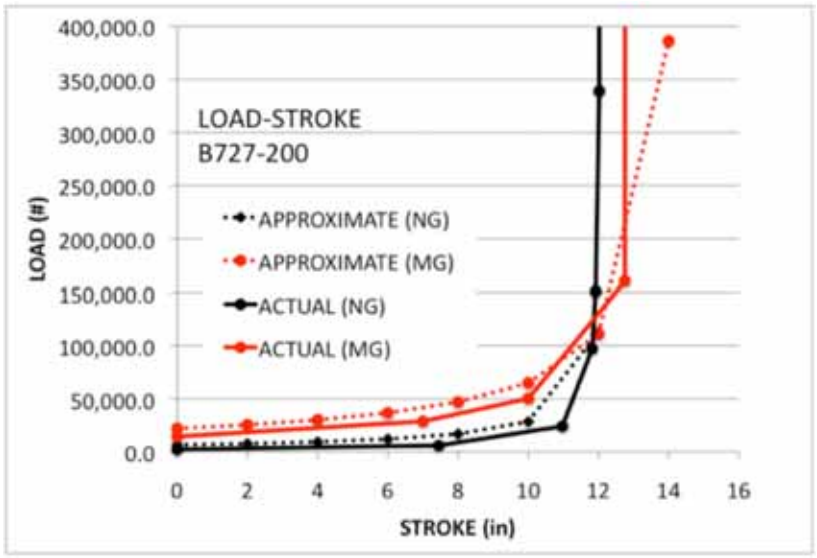

Figure 6.4. B727 Load-Stroke Behavior Comparing Approximate and Actual

The approximate approach discussed in this section is used to develop the load-stroke behavior for the four aircraft in this study (B737, B747, B757, and B767) in Figure 6.5. Load-stroke values derived from these curves were used as input for the SGAS analysis by entering strut load at incremental stroke values.

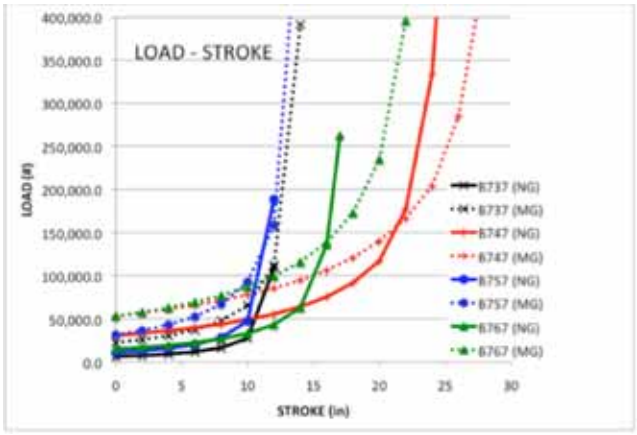

Figure 6.5. Load-Stroke Behavior used as SGAS Input

6.6 Strut Damping

For strut damping, the study aircraft were categorized with the Gerardi aircraft based on total gross weight, Table 6.5. Study aircraft were assigned a damping coefficient value for the nose and main landing gear similar to the corresponding Gerardi aircraft damping coefficient value. The damping coefficients for the Gerardi aircraft types were calculated using equation (5.13) assuming low stroke velocity.

Table 6.5. Aircraft Damping Factor Coefficient

	A	B	C	D	E
AIRCRAFT	DC-9-41	B727-200	B707-320C	DC-10-10	B747-200
GROSS WT. (lb)	114000	184800	333600	430000	775000
MAX VERT LOAD (lb)					
NG (BRAKING)	17220	25600	51770	84959	135700
MAX VERT LOAD					
MG (AFT)	53817	87800	157000	213680	183800
					28.3
DAMPING COEFF					
NG (lb/(in/sec)^2)	0.29	3.33	3.14	37.25	9.9
MG (lb/(in/sec)^2)	0.51	3.81	17.34	41.33	9.13
MG2 (lb/(in/sec)^2)					13.79
	B737-900ER	B747-400ER	B757-300	B767-400ER	
similar aircraft WT	(B)	(E)	(B)	(D)	
GROSS WT. (lb)	171000	910000	270000	450000	
MAX VERT LOAD (lb)					
NG (BRAKING)	24810	122400	42800	59650	
MG (AFT)	88993	213600	125500	211850	
DAMPING COEFF					
NG (lb/(in/sec)^2)	4	10	4	10	
MG (lb/(in/sec)^2)	4	10	4	10	

Chapter 7
Arrestor Bed Description

An arrestor bed is located within the runway safety area positioned to maximize the distance between the threshold and the arrestor bed entry. The EMAS is positioned at a setback distance from the runway threshold to avoid deterioration due to jet blast, obstruction during an undershoot, and aircraft intrusion during a low velocity overrun. The runway pavement within the RSA is used to support the EMAS. The width of the EMAS is the same as the runway and configured with steps along the EMAS sides and end to provide for emergency vehicle access. A rigid lead-in ramp is used to improve aircraft behavior at the arrestor bed entry. The EMAS is constructed using adjoining low-density concrete blocks and constant EMAS thickness is used within the EMAS cross-section. Conversely, in the longitudinal direction, the thickness is a function of minimizing aircraft stopping distance while limiting maximum deceleration to an acceptable level (1g) for passenger safety while considering the host aircraft fleet. The EMAS configuration used as a basis in this study is shown in Figure 7.1. The configuration uses a 200-ft setback with a 100-ft rigid lead-in ramp. The lead-in ramp is sloped to 3-in at the arrestor bed entry. The arrestor bed starts with a 9-in thickness and increases to 24-in over 140-ft material length. A constant bed thickness is used over the next 140-ft. At 280-ft from the arrestor bed start, the bed thickness slopes to increase the bed thickness to 30-in over 24-ft. A multiple thickness arrestor bed is used to stop an array of aircraft while limiting deceleration and drag forces to acceptable values.

The EMAS is a passive system and therefore develops aircraft deceleration through drag forces developed from tire-EMAS material interaction. Drag forces are a function of tire penetration. To maximize tire penetration, a crushable material is used. Although multiple concrete strengths can be used, for this sensitivity study a single low-density concrete material is used for the entire arrestor bed. Material behavior of the low-density concrete is shown in Figure 7.2. In addition to the stress-strain behavior of the "base" material, two modified materials are shown modifying the base material strength by an increase of 20% and by a 20% decrease. The graphs show typical crushable material behavior. Although low strain, <0.2, is not shown, the material will exhibit a strain increase in response to an increase in stress. Beyond yielding, the material exhibits

a large strain increase at a nominally constant stress. This behavior is shown in Figure 7.2 within the 0.2 to 0.5 strain range. Beyond 0.5, additional stress is required to develop larger strains. As the material approaches a fully crushed state, a substantial stress increase is required to develop marginal strain increases.

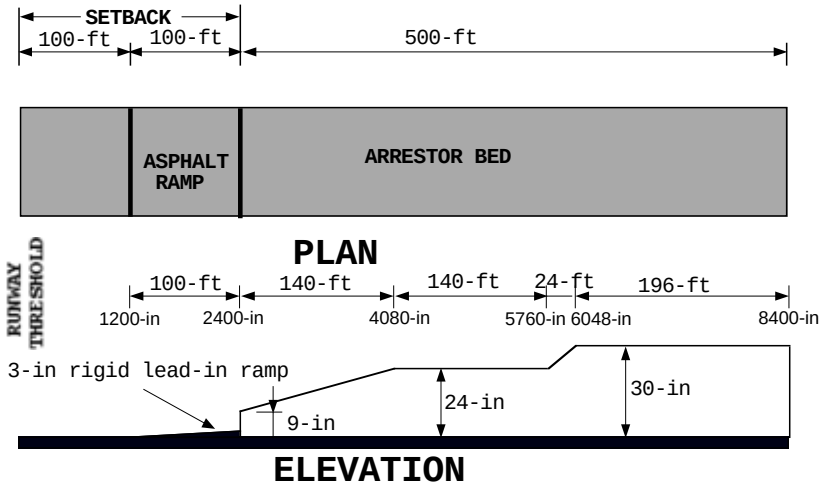

Figure 7.1. Arrestor Bed Configuration

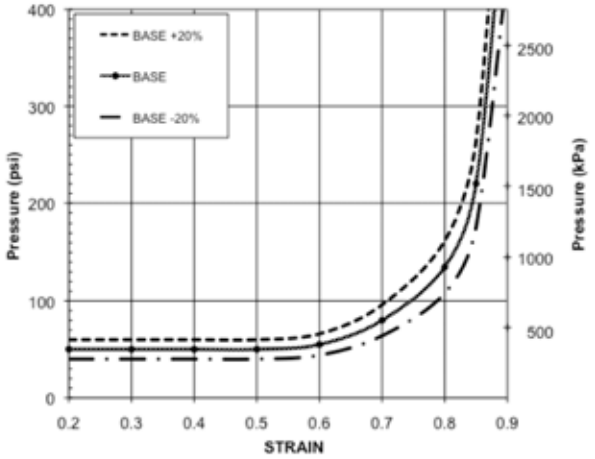

Figure 7.2. Low-Density Concrete Material Behavior

Chapter 8
SGAS Calibration

The SGAS computer code was calibrated with the FAA ARRESTOR code using the results for a B727 aircraft. Using Figure 4.2, θ_1, the location of the first tire spring was varied in SGAS until a similar B727 stopping distance was attained for both SGAS and ARRESTOR. Similar results (SGAS = 621.5-ft & ARRESTOR= 621.5-ft) were attained when θ_1 was set at 17.5° and tire springs were spaced at $\Delta\theta = 2.5°$. Comparison of the stopping distance from analyses using the two codes is shown in Figure 8.1. The aircraft undergoes constant deceleration, approximately, equal to the tire-pavement friction coefficient, before entering the arrestor bed at distance equal to 200-ft, Figure 8.1. Both analyses were conducted using 0.02 tire-pavement friction coefficient. At 200-ft, the aircraft enters the arrestor bed. The drag forces developed through arrestor material-nose gear tire interaction cause an increase in deceleration, Figure 8.2, and consequently a steeper velocity slope in Figure 8.1. The distance between the B727-200 nose gear and main gear is 63-ft. A significant deceleration increase occurs when the main gear enter the arrestor bed, approximately at a distance equal 263-ft. Beyond 263-ft, deceleration increases as a function of arrestor bed thickness and tire penetration. Beyond 400-ft, the aircraft has attained maximum tire penetration and deceleration remains fairly stable. A comparison of strut forces using the two codes, ARRESTOR and SGAS, is shown in Figure 8.3 for nose gear forces and Figure 8.4 for main gear forces. Strut behavior at the nose gear and main gear cause the cyclic force behavior shown in Figures 8.3 and 8.4 after the aircraft enters the arrestor bed.

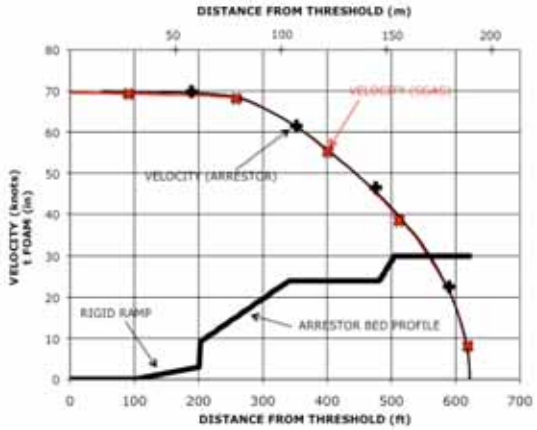

Figure 8.1. SGAS Calibration with ARRESTOR Using Stopping Distance

Even with some unknown aircraft parameter differences, a good correlation is identified between the two computer analyses for the B727 simulation.

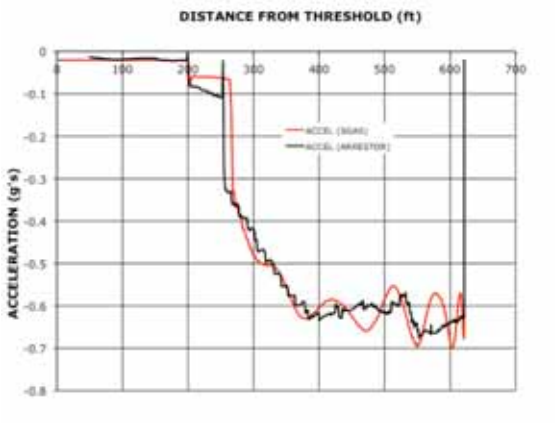

Figure 8.2. SGAS Comparison with ARRESTOR for Aircraft Deceleration

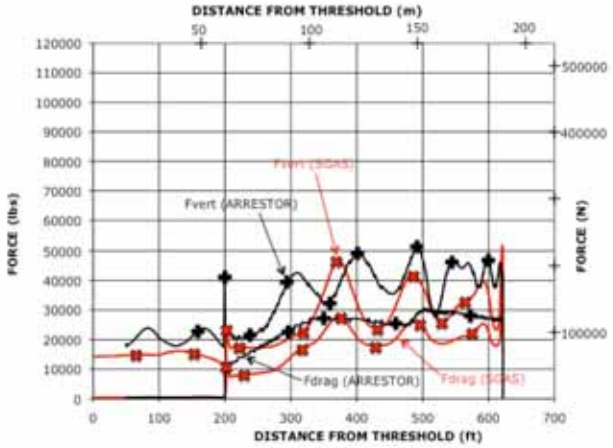

Figure 8.3. SGAS Comparison with ARRESTOR for Nose Gear Strut Forces

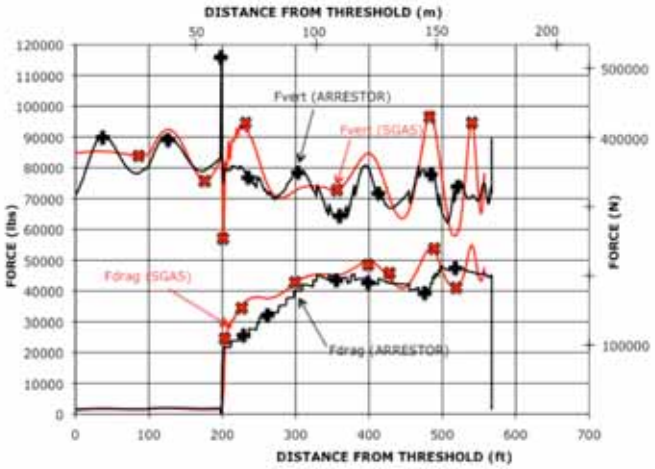

Figure 8.4. SGAS Comparison with ARRESTOR for Main Gear Strut Forces

Chapter 9
Sensitivity Analysis

9.1 Aircraft Stopping Distance Varying Arrestor Material Strength

Stopping Distance is calculated for the four aircraft types (B737, B747, B757, and B767) using the aircraft parameters included in Table 9.1, the Figure 7.1 EMAS configuration, and the base material stress-strain material behavior shown in Figure 7.2. In addition, the base material is varied by ±20% to investigate stopping distance sensitivity to material strength. Results of the analyses are shown in Figure 9.1 where stopping distance is measured from the arrestor bed entry. The heaviest aircraft, B747, has the greatest stopping distance. Each aircraft type shows that an increase in material strength by +20% decreases stopping distance and a 20% material strength decrease results in an increase in stopping distance. Consequently, for the considered aircraft, tire penetration is not a problem and drag forces increase as the material strength increases.

Table 9.1 Study Aircraft Parameters

AIRCRAFT TYPE		B727-200	B737-900ER	B747-400ER	B757-300	B767-400ER
GROSS WEIGHT	lb	184,800	171,000	910,000	270,000	450,000
(MTOW)	N	822,360	760,950	4,049,500	1,201,500	2,002,500
MOM. of INERTIA	lb in sec^2	62,800,000	42,800,000	646,300,000	120,900,000	244,700,000
(about pitch axis)	kg*m^2	7,093,260	4,834,260	72,999,585	13,655,655	27,638,865
LANDING GEAR FOOTPRINT						
NG (# TIRES)		2	2	2	2	2
MG CONFIG		DUAL	DUAL	DUAL TANDEM	DUAL TANDEM	DUAL TANDEM
NG-CG DIST	ft (m)	59.79 (18.23)	50.70 (15.46)	75.60 (23.05)	66.00 (20.12)	77.25 (23.55)
CG-MG1 DIST	ft (m)	3.23 (0.98)	5.63 (1.72)	3.36 (1.02)	7.33 (2.23)	8.58 (2.62)
CG-MG2 DIST	ft (m)			13.44 (4.10)		
NG HEIGHT	ft (m)	10.00 (3.05)	9.37 (2.86)	17.45 (5.32)	13.49 (4.11)	14.91 (4.55)
MG1 HEIGHT	ft (m)	11.42 (3.48)	9.63 (2.94)	17.60 (5.37)	13.48 (4.11)	15.29 (4.66)
MG2 HEIGHT	ft (m)			17.60 (5.37)		
NOSE GEAR STRUT						
NG Tire Width	in (mm)	11.5 (292)	7.75 (197)	20.0 (508)	13.0 (330)	14.0 (356)
NG Tire Pressure	psi (kPa)	100 (689)	185 (1275)	190 (1309)	136 (937)	185 (1275)
NG Tire Stiffness	lb/in (N/mm)	4297 (753)	5100 (894)	10700 (1875)	4400 (771)	6500 (1139)
EQUIV. SPRING C1	lb/in (N/mm)	407.0 (17.3)	482.7 (84.6)	948.1 (166.1)	430.5 (75.4)	688.2 (120.6)
EQUIV. SPRING C2	lb/in^2 (N/mm^2)	-47.0 (-0.324)	-62.8 (-0.433)	-47.8 (-0.330)	-39.1 (-0.270)	-55.5 (0.383)
UNSPRUNG STRUT WT.	lb (N)	495 (2203)	248 (1104)	1224 (5447)	428 (1905)	597 (2657)
MAIN GEAR STRUT						
MG Tires Radius	in (mm)	24.5 (622)	22.25 (565)	25.0(635)	20.0 (508)	25.0 (635)
MG Tire Width	in (mm)	17.0 (432)	16.50 (419)	20.0 (508)	14.5 (368)	20.0 (508)
MG Tire Pressure	psi (kPa)	158 (1089)	205 (1412)	230 (1585)	195 (1344)	215 (1481)
MG Tire Stiffness	lb/in (N/mm)	10370(1817)	10700 (1875)	12700 (2225)	9000 (1577)	11900 (2085)
EQUIV. SPRING C1	lb/in (N/mm)	899.7 (157.6)	921.8 (161.5)	1126.5 (197.4)	732.8 (128.4)	1058.5 (185.5)
EQUIV. SPRING C2	lb/in^2 (N/mm^2)	-58.8 (-0.406)	-62.3 (-0.430)	-57.5 (-0.397)	-48.9 (-0.337)	-55.8 (-0.385)
UNSPRUNG STRUT WT.	lb (N)	1363 (6065)	1780 (7921)	4272 (19010)	2510 (11170)	4237 (18855)

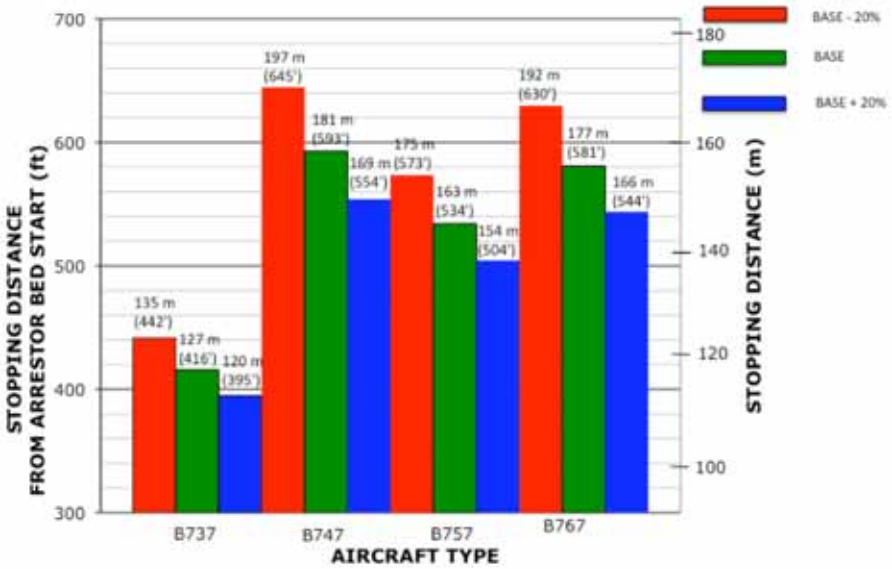

Figure 9.1 Aircraft Stopping Distance as a Function of Material Variability

9.2 Stopping Distance as a Function of Arrestor Bed Geometry

The arrestor bed is designed to have a geometry that minimizes stopping distance for the potential aircraft fleet usage while considering passenger safety and aircraft landing gear damage. In addition to the base arrestor bed geometry shown in Figure 7.1, two other EMAS geometries were investigated to compare stopping distance as a function of bed thickness. Design 1 in Figure 9.2 is the base EMAS configuration earlier shown in Figure 7.1. It uses an EMAS geometry that has a 30-in maximum bed thickness. Conversely, Design 2 has a maximum bed thickness of 24-in and Design 3 has a maximum bed thickness of 18-in, as shown in Figure 9.2. The stopping distances for the considered aircraft are shown in Figure 9.2 where stopping distance is measured from the EMAS entry. The stopping distance range is included on Figure 9.2 for easier comparison between the aircraft types and to illustrate the significance of arrestor bed thickness on stopping distance. Stopping distance is smallest for Design 1, maximum bed thickness, and largest for Design 3, minimum bed thickness. Figure 9.2 shows that the heaviest aircraft type, B747, requires the longest arrestor bed. Considering the B747 aircraft, the aircraft stopping distance increases from 593-ft in Design 1 to 614-ft in Design 2, a 3.5% stopping distance increase. Conversely, the B747 stopping distance

increases from 593-ft in Design 1 to 656-ft in Design 3, a 10.6% increase. Assuming the same "w" constant bed thickness for all three EMAS designs, to stop the B747 aircraft, Design 1 requires 749*w-ft^3 arrestor bed material. Conversely, Design 2 and Design 3 require 740.5*w-ft^3 and 652.5*w-ft^3 material, respectively. Consequently, a 1.1 % decrease in material from Design 1 to Design 2 results in a 3.5% increase in stopping distance. A 12.9% decrease in material from Design 1 to Design 3 results in a 10.6% stopping distance increase.

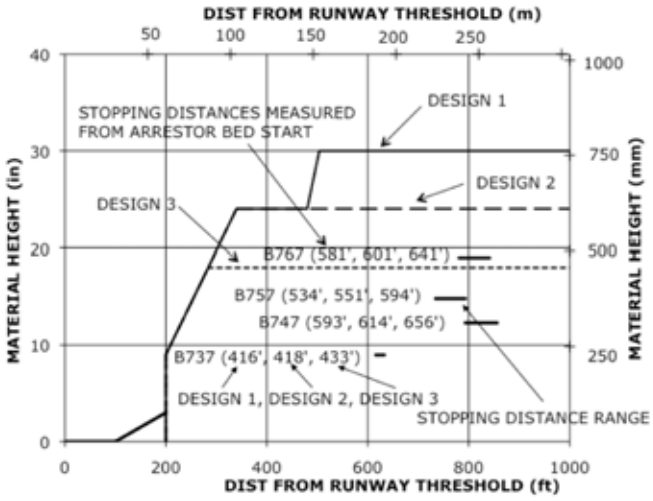

Figure 9.2 Aircraft Stopping Distance as a Function of EMAS Geometry

9.3 Stopping Distance Considering Multiple Low-Density Concrete Mixes

In addition to the low-density concrete mix previously discussed, BASE, stress-strain behavior for five low-density concrete mixes are shown in Figure 9.3. Only large strain behavior is shown. The five mixes are representatives of the multiple concrete mixes developed during this study. A description of the mixes is included in the thesis by Marisetty (Marisetty et al., 2008). Each mix shows typical crushable material behavior; after the material attains a limiting stress value, $\sigma_{crushing}$, the material exhibits large strain increase with minimal stress increase. The crushing stress for the considered mixes ranges from 38 psi to 110 psi. At approximately 0.85 strain, all mixes experienced strain hardening where a significant increase in stress was required to cause a minimal strain increase.

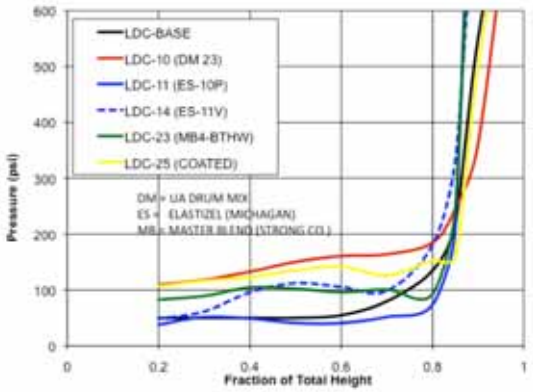

Figure 9.3 Drum Mix Stress-Strain Material Behavior

Stopping distance results for the five mixes, plus BASE, are shown in Figure 9.4 where stopping distance in the figure is measured from the EMAS entry. In addition, the maximum deceleration that each aircraft experiences while moving through the EMAS is shown for each case. All of the decelerations are below 1.0 g and consequently within acceptable maximum deceleration limits. Figure 9.4 shows that aircraft stopping distance is highly sensitive to the concrete mix used. The B737 experienced minimum stopping distance, 341-ft, using the lowest yield stress mix, ES-10P ($\sigma_{crushing}$= 38.3 psi). Conversely, the shortest stopping distance for the other aircraft types occurred using MB4-BTHW ($\sigma_{crushing}$= 89.6 psi). Table 9.2 lists stopping distance as a function of

concrete mix and aircraft. The mixes are ordered based on crushing stress, $\sigma_{crushing}$, from low, $\sigma_{crushing}$ = 38.3 psi, to high, $\sigma_{crushing}$ = 109.6 psi. A stopping distance trend based on crushing stress in Table 9.2 is unidentifiable. Consequently, to minimize stopping distance both tire penetration and arrestor material strength needs to be considered.

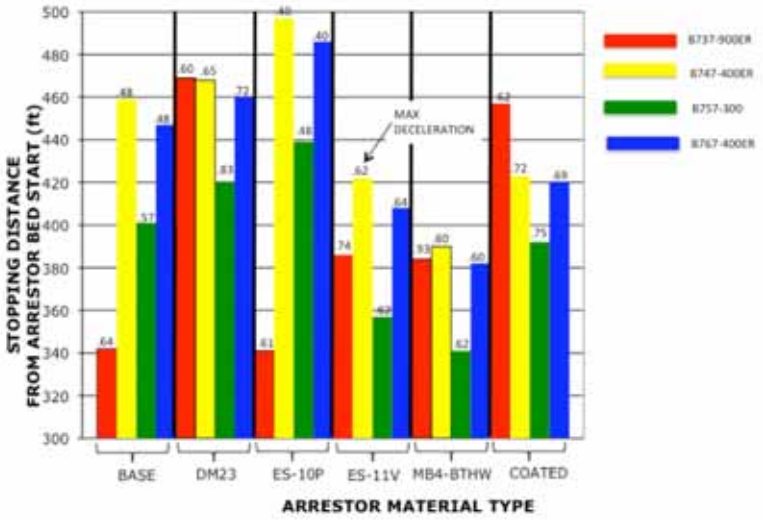

Figure 9.4 Stopping Distance as a Function of Drum Mix

Table 9.2 Stopping Distance Organized Based on Drum Mix Crushing Strength

MIX TYPE	CRUSHING STRESS	STOPPING DISTANCE (ft)			
	(psi)	B737	B747	B757	B767
LDC-11 (ES-10P)	38.3	341	497	439	486
LDC-14 (ES-11V)	48.5	386	422	357	408
LDC -BASE	50.0	342	459	401	447
LDC-23 (MB4-BTHW)	89.6	384	390	341	382
LDC-25 (COATED)	107.0	457	423	392	420
LDC-10 (DM-23)	109.6	469	468	420	460

Chapter 10
Conclusions

Four aircraft types were considered in this study to investigate aircraft stopping distance as a function of aircraft type, EMAS geometry, and concrete mix. During this study, the computer code SGAS was developed. The SGAS code provides a method to analyze current aircraft types included in an airport's aircraft fleet using aircraft parameters that can be derived by the SGAS user. In addition, four boilerplate Excel files were developed to transform ARRESTOR analysis output data and SGAS analysis output data for graphical presentation. An approach has been presented to develop aircraft parameters warranted in a SGAS analysis. In concrete mixes with low crushing stress (<100 psi), the heaviest aircraft type, B747, is the critical aircraft. When material crushing stress exceeds 100 psi, the lightest aircraft type, B737, becomes the critical aircraft because of tire penetration. Stopping distance decreases as the arrestor bed thickness increases. Consequently, a methodology has been presented to investigate aircraft stopping distance for various aircraft in order to optimize an EMAS as a function of available space, permissible deceleration, and economics.

References

Boeing Company. (2005a). "737 Airplane Characteristics for Airport Planning." www.boeing.com/commercial/airports/plan_manuals.html (September 15, 2008).

Boeing Company. (2005b). "767 Airplane Characteristics for Airport Planning." www.boeing.com/commercial/airports/plan_manuals.html (September 15, 2008).

Boeing Company. (2002a). "747-400 Airplane Characteristics for Airport Planning." www.boeing.com/commercial/airports/plan_manuals.html (May 26, 2006).

Boeing Company. (2002b). "757-200/300 Airplane Characteristics for Airport Planning." www.boeing.com/commercial/airports/plan_manuals.html (September 15, 2008).

Boeing Company. (1985). "727 Airplane Characteristics for Airport Planning." www.boeing.com/commercial/airports/plan_manuals.html (September 15, 2008).

Cook, R.F., Teubert, C.A., and Hayhoe, G. (1995), "Soft Ground Arrestor Program," U.S. Department of Transportation Federal Aviation Administration, DOT/FAA/CT-95.

Cook, R.F. (1985), "Aircraft Operation on Soil Prediction Techniques," Grouping 1: Volume 1, Discussion," University of Dayton Research Institute, Final Report, UDR-TR-83-127.

Curry, N.S. (1988), *Aircraft Landing Gear Design: Principles and Practices*, AIAA, Washington.

David, R.E. (1990). "Location of Commercial Aircraft Accidents / Incidents Relative to Runways," Federal Aviation Administration, Washington, DC, 1990.

Federal Aviation Administration (2009). "Fact Sheet Engineered Material Arresting System (EMAS)," www.faa.gov/news/fact_sheets/news_story.cfm?newsId=6279, (September 25, 2009).

Federal Aviation Administration (2005). "Advisory Circular 150/5220-22A, Engineered Materials Arresting System (EMAS) for Aircraft Overrun." U.S. Department of Transportation Federal Aviation Administration.

Federal Aviation Administration (2004). "Financial Feasibility and Equivalency of Runway Safety Area Improvements and Engineered Material Arresting Systems," U.S. Department of Transportation Federal Aviation Administration.

Gerardi, A.G. (1977). Collection of Commercial Aircraft Characteristics for Study of Runway Roughness, Technical Report FAA-RD-76-64, U.S. Air Force Engineering and Services Center, Tyndall Air Force Base, FL.

Google Earth, (2009), 34˚44’07.21”N 92˚12’02.83”W.

Hall, J., Ayres, M., and Wong, D. (2008). “Analysis of Aircraft Overruns and Undershoots for Runway Safety Areas,” ACRP Report 3, Transportation Research Board, Washington, D.C.

Kirkland, I.D. and Caves, R.E. (2002). “New Aircraft Overrun Database, 1980-1998,” Transportation Research Record, Washington, DC, #1788, pp 93-100.

Lautenberg, F.R. (2006). “An Accident Waiting to Happen: Over Half of America’s Airports Have Runways that Fail to Meet FAA Standards,” Report by the Office of Senator Frank R. Lautenberg.

Marisetty, S.C., Bailey, E.D., Hale, W.M., and Heymsfield, E. (2008), Development of a Soft Ground Arrestor System, Mack-Blackwell Transportation Center, Final Report, MBTC-2089.

Phillips, N.S. and Cook, R.F. (1983). *Aircraft Operation on Soil Surfaces, Computer Routine Revisions and Improvements, Volume 1,* (Technical Report ESL-82-29) U.S. Air Force Engineering and Services Center, Tyndall Air Force Base, FL.

Appendix A
SGAS Input

SGAS Run File

```
3
!problem 1, base material properties
sgasb747.in
sgasb747.plt
!problem 2, base - 20% material properties
sgasb747.in-20
sgasb747.plt-20
!problem 3, base + 20% material properties
sgasb747.in+20
sgasb747.plt+20
```

SGAS Input File

```
! CHECK SGAS CODE WITH ARRESTOR USING A B747 AIRCRAFT
! TYPE OF AIRCRAFT (# OF MAIN GEAR = 4 (B747); = 2 (OTHER))
B747
!DT TMAX XN (INITIAL NG POSITION, IN)
!0.0005 12.0 1063.8
0.0005 14.0 0.0
! GW, IXX,IYY,IZZ, GRAVITY
! TOTAL AIRCRAFT MASS MOMENT OF INERTIA
910000. 4.0E+08 6.463E+08 4.0E+08 386.0
! INITIAL VELOCITY XD,YD,ZD
1410.0 0.0 0.0
!ANGLE_ROLL, ANGLE_PITCH, ANGLE_YAW
0.0 0.0 0.0
!ANGLEVEL_ROLL, ANGLEVEL_PITCH, ANGLEVEL_YAW
0.0 0.0 0.0
! ANGLEACC_PITCH, INITIAL PITCH ANGLE ACCELERATION (CW = +), RADIANS
!0.80
0.00
! THRUST
00.0
!
! NOSE GEAR DATA
!WT_NG, XDIST_NG, ZDIST_NG, GAMN
1224.0 907.2 209.4 0.0
!NOSE GEAR TIRE
! NTIRE_NG, NTIREfrnt_NG,TIRERADIUS_NG,TIREWIDTH_NG,SECHN,TIRESTIFF_NG,C1N,C2N, SURFMUN
!C1N and C2N are based on theata(start) = 20degs and theata(end) = 120 degs
2 2 25.0 20.00 100.0 10700.0 948.1 -47.8 0.02
! STRUT INFORMATION - NOSE GEAR
! STRUT PNEUMATIC FORCE - STROKE RELATION
!# OF STROKE VALUES, NSTROKEVAL_NG
14
! STROKE VALUES
0.0 2.0 4.0 6.0 8.0 10.0 12.0 14.0 16.0 18.0 20.0 22.0 24.0 25.0
! CORRESPONDING PNEUMATIC FORCE
30600.0 33108.0 36045.0 39532.0 43739.0 48916.0 55440.0 63918.0 75381.0 91741.0 116990.0 177300.0 334022.0 538715.0
!HYDRAULIC DAMPING COEFFICIENT FOR POSITIVE STROKE VEL (DAMPCOEF_NGposSD), HYDRAULIC DAMPING COEFFICIENT FOR NEGATIVE STROKE VEL
(DAMPCOEF_NGnegSD)
10.0 10.0
! MAIN GEAR DATA: WING
!WT_MG, XDIST_MG,YDIST_MG,ZDIST_MG,GAMM,ETA, PHI
4272.0 40.3 216.5 211.2 0.00 0.0 0.0
!MAIN GEAR TIRE: WING
!NTIRE_MG, NTIREfrnt_MG,TIRERADIUS_MG,TIREWIDTH_MG,SECHM,TIRESTIFF(MG),C1M,C2M,SURFMUM
!C1N and C2N are based on theata(start) = 20degs and theata(end) = 120 degs
4 2 25.00 20.00 100.0 12700.0 1126.5 -57.5 0.02
! STRUT INFORMATION - MAIN GEAR WING
! STRUT PNEUMATIC FORCE - STROKE RELATION
!# OF STROKE VALUES, NSTROKEVAL_MG
16
! STROKE VALUES MG_STROKE(IGEAR,I)
0.0 2.0 4.0 6.0 8.0 10.0 12.0 14.0 16.0 18.0 20.0 22.0 24.0 26.0 28.0 30.0
! CORRESPONDING PNEUMATIC FORCE MG_PNEUFORCE(IGEAR,I)
53400.0 57000.0 61098.0 65808.0 71276.0 77703.0 85363.0 94650.0 106143.0 120736.0 139877.0 166085.0 204160.0 285048.0 456139.0 940110.0
!HYDRAULIC DAMPING COEFFICIENT FOR POSITIVE STROKE VEL (DAMPCOEF_MGposSD), HYDRAULIC DAMPING COEFFICIENT FOR NEGATIVE STROKE VEL
(DAMPCOEF_NGnegSD)
10.0 10.0
! MAIN GEAR DATA: BODY
!WT_MG, XDIST_MG,YDIST_MG,ZDIST_MG,GAMM,ETA, PHI
4272.0 161.3 75.5 211.2 0.00 0.0 0.0
!MAIN GEAR TIRE
!NTIRE_MG, NTIREfrnt_MG,TIRERADIUS_MG,TIREWIDTH_MG,SECHM,TIRESTIFF(MG),C1M,C2M,SURFMUM
!C1N and C2N are based on theata(start) = 20degs and theata(end) = 120 degs
4 2 25.00 20.00 100.0 12700.0 1126.5 -57.5 0.02
! STRUT INFORMATION - MAIN GEAR BODY
! STRUT PNEUMATIC FORCE - STROKE RELATION
!# OF STROKE VALUES, NSTROKEVAL_MG BODY
15
! STROKE VALUES MG_STROKE(IGEAR,I)
0.0 2.0 4.0 6.0 8.0 10.0 12.0 14.0 16.0 18.0 20.0 22.0 24.0 26.0 28.0 30.0
! CORRESPONDING PNEUMATIC FORCE MG_PNEUFORCE(IGEAR,I)
53400.0 57000.0 61098.0 65808.0 71276.0 77703.0 85363.0 94650.0 106143.0 120736.0 139877.0 166085.0 204160.0 285048.0 456139.0 940110.0
!HYDRAULIC DAMPING COEFFICIENT FOR POSITIVE STROKE VEL (DAMPCOEF_MGposSD), HYDRAULIC DAMPING COEFFICIENT FOR NEGATIVE STROKE VEL
(DAMPCOEF_NGnegSD)
10.0 10.0
!ARRESTOR BED GEOMETRY AND MATERIAL INPUT
!NUMBER OF ARRESTOR BED SECTIONS
6
! ARRESTOR BED SECTION 1
!XSTART(1) HTSTART(1) XEND(1) HTEND(1)
0.0 0.0 1200.0 0.0
!NUMBER OF STRAIN VALUES NSTRAINVAL(ISECT=1)
12
! STRAIN VALUES TO DESCRIBE MATERIAL BEHAVIOR STRAINVAL_INPT(ISECT,I)
0.0 0.10 0.20 0.30 0.40 0.50 0.60 0.70 0.80 0.85 0.90 1.0
! STRESS VALUES TO DESCRIBE MATERIAL BEHAVIOR STRESSVAL_INPT(ISECT,I) (USE 1000.0 FOR RIGID PAVEMENT)
1000.0 1000.0 1000.0 1000.0 1000.0 1000.0 1000.0 1000.0 1000.0 1000.0 1000.0 1000.0
! ARRESTOR BED SECTION 2
!XSTART(2) HTSTART(2) XEND(2) HTEND(2)
1200.0 0.0 2400.0 3.0
!NUMBER OF STRAIN VALUES NSTRAINVAL(ISECT=2)
12
```

```
! STRAIN VALUES TO DESCRIBE MATERIAL BEHAVIOR STRAINVAL_INPT(ISECT,I)
0.0 0.10 0.20 0.30 0.40 0.50 0.60 0.70 0.80 0.85 0.90 1.0
! STRESS VALUES TO DESCRIBE MATERIAL BEHAVIOR STRESSVAL_INPT(ISECT,I) (USE 1000.0 FOR RIGID PAVEMENT)
1000.0 1000.0 1000.0 1000.0 1000.0 1000.0 1000.0 1000.0 1000.0 1000.0 1000.0 1000.0
! ARRESTOR BED SECTION 3
!XSTART(3) HTSTART(3) XEND(3) HTEND(3)
2400.0 9.0 4080.0 24.0
!NUMBER OF STRAIN VALUES NSTRAINVAL(ISECT=3)
12
! STRAIN VALUES TO DESCRIBE MATERIAL BEHAVIOR STRAINVAL_INPT(ISECT,I)
0.0 0.10 0.20 0.30 0.40 0.50 0.60 0.70 0.80 0.85 0.90 1.0
! STRESS VALUES TO DESCRIBE MATERIAL BEHAVIOR STRESSVAL_INPT(ISECT,I) (USE 1000.0 FOR RIGID PAVEMENT)
0.0 25.0 50.0 50.0 50.0 50.0 55.0 80.0 135.0 220.0 550.0 1000.0
! ARRESTOR BED SECTION 4
!XSTART(4) HTSTART(4) XEND(4) HTEND(4)
4080.0 24.0 5760.0 24.0
!NUMBER OF STRAIN VALUES NSTRAINVAL(ISECT=4)
12
! STRAIN VALUES TO DESCRIBE MATERIAL BEHAVIOR STRAINVAL_INPT(ISECT,I)
0.0 0.10 0.20 0.30 0.40 0.50 0.60 0.70 0.80 0.85 0.90 1.0
! STRESS VALUES TO DESCRIBE MATERIAL BEHAVIOR STRESSVAL_INPT(ISECT,I) (USE 1000.0 FOR RIGID PAVEMENT)
0.0 25.0 50.0 50.0 50.0 50.0 55.0 80.0 135.0 220.0 550.0 1000.0
! ARRESTOR BED SECTION 5
!XSTART(5) HTSTART(5) XEND(5) HTEND(5)
5760.0 24.0 6048.0 30.0
!NUMBER OF STRAIN VALUES NSTRAINVAL(ISECT=5)
12
! STRAIN VALUES TO DESCRIBE MATERIAL BEHAVIOR STRAINVAL_INPT(ISECT,I)
0.0 0.10 0.20 0.30 0.40 0.50 0.60 0.70 0.80 0.85 0.90 1.0
! STRESS VALUES TO DESCRIBE MATERIAL BEHAVIOR STRESSVAL_INPT(ISECT,I) (USE 1000.0 FOR RIGID PAVEMENT)
0.0 25.0 50.0 50.0 50.0 50.0 55.0 80.0 135.0 220.0 550.0 1000.0
! ARRESTOR BED SECTION 6
!XSTART(6) HTSTART(6) XEND(6) HTEND(6)
6048.0 30.0 12000.0 30.0
!NUMBER OF STRAIN VALUES NSTRAINVAL(ISECT=6)
12
! STRAIN VALUES TO DESCRIBE MATERIAL BEHAVIOR STRAINVAL_INPT(ISECT,I)
0.0 0.10 0.20 0.30 0.40 0.50 0.60 0.70 0.80 0.85 0.90 1.0
! STRESS VALUES TO DESCRIBE MATERIAL BEHAVIOR STRESSVAL_INPT(ISECT,I) (USE 1000.0 FOR RIGID PAVEMENT)
0.0 25.0 50.0 50.0 50.0 50.0 55.0 80.0 135.0 220.0 550.0 1000.0
```